Microstructure evolution and thermal properties in nanocrystalline Cu during mechanical attrition

Y. H. Zhao* and K. Lu
Shenyang National Laboratory for Materials Science, Institute of Metal Research, Chinese Academy of Sciences, Shenyang 110015, People's Republic of China

K. Zhang
Department of Physics, University of Hamburg, D-20146, Hamburg, Germany
(Received 15 January 2002; revised manuscript received 25 March 2002; published 5 August 2002)

The microstructural evolution and thermal properties of nanocrystalline (nc) Cu during mechanical attrition were investigated by using quantitative x-ray-diffraction and thermal analysis techniques. Upon milling of the Cu powders with coarse grains, the grain sizes are found to decrease gradually with the milling time, and remain unchanged at a steady-state value (about 11 nm) with continued milling. The microstrain and the stored enthalpy increase to maximum values during the grain refinement, and decrease then increase to the second maxima and decrease again within the milling stage of steady-state grain size, while the lattice parameter remains unchanged during the entire milling process. The grain boundary (GB) enthalpy of the nc Cu was estimated, showing a GB softening-hardening-softening cyclic variation within the steady-state milling. The present work indicated with clear experimental evidence that even within the milling stage of steady-state grain size, the microstructure (both the GB's and the crystallites) of nc materials is still changing, which may result from the GB sliding.

DOI: 10.1103/PhysRevB.66.085404 PACS number(s): 61.72.Dd, 61.46.+w, 65.40.Gr, 81.20.Wk

I. INTRODUCTION

In last decade, nanocrystalline (nc) materials have attracted increasing scientific interest because of their unusual properties that are normally attributed to the ultrafine grains and the large amounts of grain boundaries (GB's).[1] Mechanical attrition by ball milling has been widely used in laboratory research to synthesize nc materials due to its simplicity, low cost, and applicability to essentially all classes of materials.[2–5] Extensive work has been performed on the formation of nc structures by mechanical attrition of single-phase powders,[6–12] mechanical alloying of dissimilar powders,[13–15] and mechanical crystallization of amorphous materials.[16–18] Among these investigations, the microstructure evolution during mechanical attrition of single-phase materials is of significant importance to the understanding of alloy behavior and the formation mechanisms of nc structures.

In the literature, the grain size, microstrain [internal lattice root mean square (rms) strain] and stored enthalpy are often used to characterize the microstructure evolution of the milled powders. Using x-ray line broadening analysis, it is commonly found that the mean crystallite size of the milled elements decreases with the milling time, and reaches a minimum steady-state value ($D_{\min}$). An extension of milling will not be able to decrease $D_{\min}$ further.[6–12,19–21] $D_{\min}$, which was found to scale with the melting point of metals in some cases, is not yet well understood. It is obvious that $D_{\min}$ is associated with the plastic deformation mechanism and grain size stability of nc materials. Some explanations have been proposed that $D_{\min}$ is correlated with the dislocation (and other defects) activities and recoveries.[8] The variations of lattice rms strains of the milled powders are very complicated. For Ru, AlRu,[6] Al, Ag, Ni, W,[9] Fe,[9,11] etc., a maximum value is observed in the plots of rms strain as a function of the reciprocal grain size (or the milling time), whereas for the fcc elements (e.g., Pd) milled in a high-energy shaker mill,[8] only a continuous increase of lattice strain during the grain refinement is noted. The stored enthalpies of the milled powders have similar variations versus the reciprocal grain size: an increase to a maximum value then a quick decrease at $D_{\min}$.[6,8,9,11] Several suggestions have been offered to explain the maxima in rms strain and stored enthalpy, including a change in deformation mechanism from dislocation movement to GB sliding,[6] impurity pickup during milling,[6] the GB softening,[11] etc. Nevertheless, no satisfactory explanation has been found. In addition, most of the former investigations focused on the structure evolution of the milled powders during grain refinement. Very few studies were performed on the further microstructure evolution with extended milling after $D_{\min}$ was reached, which should be helpful to the understanding of the deformation mechanism of nc materials and of the maxima in rms strain and stored enthalpy. Furthermore, an evident lattice expansion was found in the milled nc Si,[20] Se,[21] and Ge.[22] However, whether the lattice expansion can exist in milled nc pure metals still needs experimental clarification. The objective of the present work is based on these considerations.

In this work, we will study the microstructure evolution and the change of the thermal properties of nc Cu during mechanical attrition, especially during the milling stage after $D_{\min}$ was reached. Microstructural parameters such as the lattice strain and lattice parameter, as well as thermal properties including the stored enthalpy of the nc Cu samples, were quantitatively measured. The dislocation density and the GB enthalpy of the milled Cu were estimated and the deformation mechanism of nc materials during attrition was explored.

II. EXPERIMENTAL PROCEDURES

A. Sample preparation

Mechanical attrition of commercial elemental Cu powders (purity 99.99% and particle size smaller than 200 mesh) was carried out in a WL-1 planetary ball mill with a working voltage of 100 V. The milling media were hardened steel balls and vial. The size of the vial was 80 mm in inner diameter and 73 mm in height, with a capacity of 367 cm^3. Balls with diameters of 20 mm (four), 16 mm (eight), and 10 mm (eight) were used. Powders of about 5-g Cu were charged into the vial with a ball-to-powder weight ratio of 60:1. To avoid oxidation, the powders were sealed in a stationary dry Ar atmosphere ($O_2, H_2 < 5$ ppm), with an overpressure of about 2 atm, by an elastomer O ring. Each mechanical attrition procedure was started with a new batch of initial powders and was carried out without interruption. The temperature of the vial was kept at ambient temperature below 323 K during the milling process by dynamic aircooling.

B. X-ray-diffraction measurements

Quantitative x-ray-diffraction (XRD) measurements of the milled Cu powders were performed on the wide-angle goniometer of a Rigaku DMAX/2400 x-ray diffractometer. The milled Cu powders used for XRD measurements were filled in the rectangle groove (with a size of $12 \times 18\ mm^2$ and a depth of 1 mm) of the sample holder. A rotating Cu target was used with a measuring voltage of 58 kV and a current of 180 mA. The divergence, antiscattering, and receiving slits were chosen to have widths of 1/2°, 1/2°, and 0.15 mm, respectively. The graphite curved single-crystal $\langle 0002 \rangle$ monochromator was used to select the Cu $K\alpha$ radiation (with wavelengths of $\lambda_{K\alpha 1} = 1.54056$ Å and $\lambda_{K\alpha 2} = 1.54439$ Å) at the goniometer receiving slit section. With these wavelengths, the extinction depth in Cu was calculated to be less than 100 μm, which was much smaller than the thickness of the measured sample. A θ-2θ scan mode was used to record the XRD pattern of the investigated samples. The scan range for 2θ was from 40° to 143°, and the experimental temperature was 293 ± 1 K. A small angular step size of $2\theta = 0.02°$ and a fixed counting time of 10 s were selected to measure the intensity of the Bragg reflections. For the rest of the XRD pattern, where only the background intensity was anticipated, a step size of 0.1° and a counting time of 5 s were used.

C. Thermal and other analyses

Thermal analysis for the milled Cu powders was performed in a Perkin-Elmer differential scanning calorimeter (DSC-7) at a constant heating rate of 10 K min^{-1}. The temperature (with an accuracy of ± 0.2 K) and energy (± 0.04 mJ s^{-1}) scales of the DSC-7 were calibrated by means of pure In and Zn standard samples. About 10–30-mg-milled Cu powder samples were contained in Al pans for each measurement. A flowing high-purity Ar atmosphere was used during each DSC run in order to prevent oxidation of the sample surface.

Transmission electron microscopy (TEM) observations were conducted on a Philips EM 420 microscope operated at an accelerating voltage of 100 kV. The milled Cu powders were first separated by ultrasonic vibration in an alcohol solution, then they were collected and supported by Cu grids for TEM observations. The composition of the milled powders was examined by means of a wet chemical analysis, and oxygen content was detected by means of LECO TC-436 O/N Analysis.

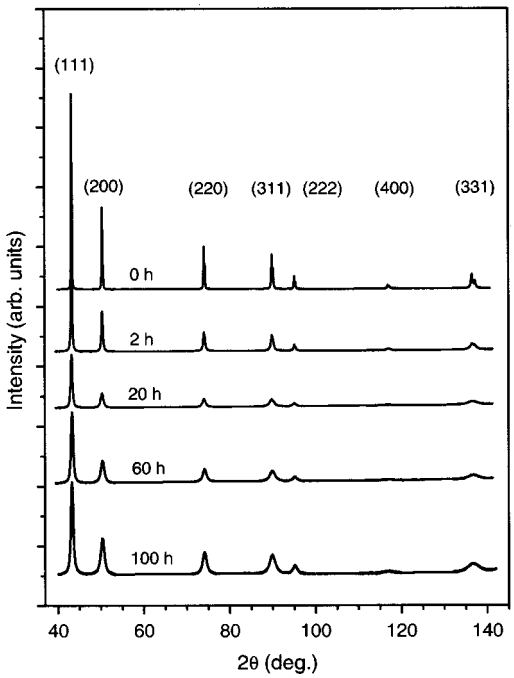

FIG. 1. The XRD lines of the milled Cu samples with different milling times (as indicated).

III. RESULTS

A. Microstructure evolution

Figure 1 shows typical XRD patterns of the Cu samples subjected to different periods of milling investigated from $2\theta = 40°$ to 143°. It is evident that, with the milling proceeding, the Bragg reflection peak intensities of the milled samples are decreased, while the peaks are significantly broadened, suggesting that large amounts of defects were introduced into the samples by attrition. Moreover, the relative peak intensities of the milled Cu samples are comparable to the standard values of Cu in JCPDS cards,[23] indicating that there is no evident texture induced into the sample during mechanical attrition.

1. Grain size and microstrain

The grain size and microstrain can be calculated from the integral width of the XRD peaks utilizing the Scherrer-Wilson equation (A detailed calculation procedure was previously described in Refs. 11 and 24),

$$\frac{\beta_{hkl}^2}{tg^2\theta_{hkl}} = \frac{\lambda \beta_{hkl}}{D_{hkl} tg\,\theta_{hkl} \sin\theta_{hkl}} + 16\langle \varepsilon_{hkl}^2 \rangle^{1/2}, \qquad (1)$$

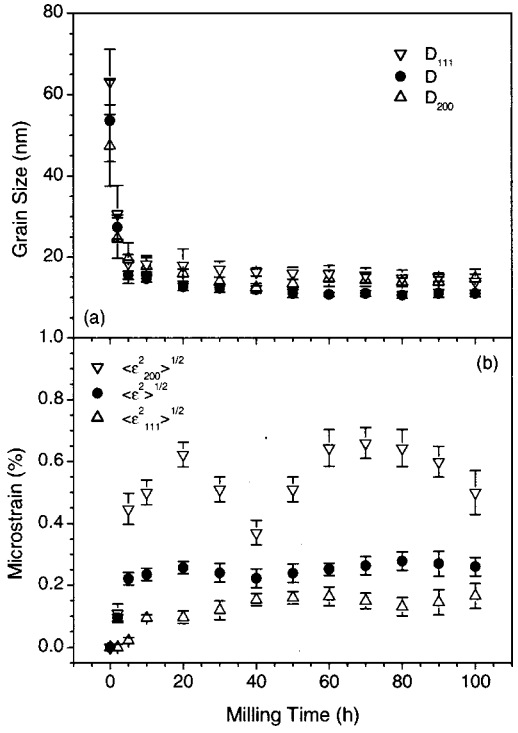

FIG. 2. Milling time dependences of the mean grain size D (a) and lattice strain $\langle\varepsilon^2\rangle^{1/2}$ (b), the grain sizes [D_{200} and D_{111} (a)] and lattice strains [$\langle\varepsilon^2_{200}\rangle^{1/2}$ and $\langle\varepsilon^2_{111}\rangle^{1/2}$, (b)] along the $\langle 200\rangle$ and $\langle 111\rangle$ directions of the milled Cu samples.

where λ is the wavelength of Cu $K\alpha 1$ irradiation, and D_{hkl} and $\langle\varepsilon^2_{hkl}\rangle^{1/2}$ represent the thickness and the mean magnitude of microstrain of the grains in the $\langle hkl\rangle$ direction, respectively. The mean grain size D and the mean lattice strain $\langle\varepsilon^2\rangle^{1/2}$ can be obtained by performing a least-square fit to $\beta^2_{hkl}/tg^2\theta_{hkl}$ plotted against $\lambda\beta_{hkl}/(tg\,\theta_{hkl}\sin\theta_{hkl})$ for all of the measured peaks. From the pairs of (111)–(222) and (200)–(400) reflections, the grain sizes and microstrains along the $\langle 111\rangle$ and $\langle 200\rangle$ directions of the milled Cu samples can be obtained.

Figures 2(a) and 2(b) show the calculated $D\langle\varepsilon^2\rangle^{1/2}$, and $D_{111}\langle\varepsilon^2_{111}\rangle^{1/2}$, as well as $D_{200}\langle\varepsilon^2_{200}\rangle^{1/2}$ of the milled Cu samples. D is found to decrease sharply from 54 ± 10 (0 h) to 15 ± 1 nm (10 h) in the early stage of milling, and remain unchanged at a steady-state value (about 11 nm) when the milling time (t) is larger than 20 h. $D_{\min}$ of the milled Cu, in the literature, was reported to be 20 nm when the ball-to-powder ratio was 10:1, and 25 nm when the ball-to-powder ratio was 5:1.[2] The different $D_{\min}$ values of the milled Cu are caused by the different milled conditions, such as the ball-to-powder ratio, etc. From Fig. 2(a), it is clear that the difference between D_{111} and D_{200} decreases evidently with increasing the milling time. For instance, when $t=0$ h, D_{200} (48 ± 10 nm) is much smaller than D_{111} (63 ± 8 nm), while when $t\geqslant 10$ h, D_{111} and D_{200} are approximately equal, suggesting that the grain shapes of the milled Cu samples turned from anisotropic to equiaxial during the milling process. A similar result was also found in milled Fe powders.[11]

The microstrain of the milled Cu is found to possess anisotropic and cyclic-change behaviors as a function of the milling time. First, during the entire milling process, $\langle\varepsilon^2_{200}\rangle^{1/2}$ is evidently larger than $\langle\varepsilon^2\rangle^{1/2}$, while $\langle\varepsilon^2_{111}\rangle^{1/2}$ is smaller than $\langle\varepsilon^2\rangle^{1/2}$, suggesting an anisotropic behavior of the microstrain. Second, with increasing milling time, $\langle\varepsilon^2_{200}\rangle^{1/2}$ increases from 0 (0 h) to a maximum value of $0.62\pm 0.04\%$ (20 h), and decreases to $0.37\pm 0.04\%$ when $t=40$ h, with the continued milling, $\langle\varepsilon^2_{200}\rangle^{1/2}$ again increases to the second maximum value of $0.66\pm 0.05\%$ (70 h) and drops to $0.50\pm 0.07\%$ at the longest milling time of 100 h. The variation of the amplitude of $\langle\varepsilon^2_{200}\rangle^{1/2}$ versus the milling time is evidently beyond the experimental uncertainty, which means that the cyclic change of $\langle\varepsilon^2_{200}\rangle^{1/2}$ cannot be neglected. $\langle\varepsilon^2\rangle^{1/2}$ exhibits a similar cyclic variation with $\langle\varepsilon^2_{200}\rangle^{1/2}$ during the milling process within the error bars. $\langle\varepsilon^2_{111}\rangle^{1/2}$, within the steady-state milling ($t\geqslant 20$ h), exhibits the inverse variation to $\langle\varepsilon^2_{200}\rangle^{1/2}$ and $\langle\varepsilon^2\rangle^{1/2}$ within the error bars.

In the literature, significantly anisotropic microstrain was observed in ultra-fine grained Cu synthesized by severe plastic deformation (SPD) technique[25] and nc Pd by consolidation of ultrafine particles[26] (UFP's): $\langle\varepsilon^2_{200}\rangle^{1/2}$ is much larger than $\langle\varepsilon^2_{111}\rangle^{1/2}$, which agrees with the present result. Similar results were also found in the nc Cu prepared by electrodeposition (ED) method.[27] Moreover, an increasing anisotropic microstrain with grain refinement was found in nc Se specimens produced by nanocrystallization of amorphous solid (NAS) method.[24] However, the cyclic variation of the microstrain versus the milling time is never reported in literature. For intermetallic compound AlRu (Ref. 6) and pure elements Ru,[6] W, Ni, Al, Ag,[9] and Fe,[11] the lattice strain is found to increase to a maximum value and then decrease with the further milling, which is similar to the first cycle of the microstrain in milled Cu ($t\leqslant 40$ h). For the elements Pd (Ref. 8) and Ti,[28] the microstrain increases monotonically with the reciprocal grain size, the variation tendency of which is similar to that of the milled Cu samples during grain refinement ($t\leqslant 20$ h). The anisotropic microstrain can be caused by the different yield stresses along different crystallographic orientations. The cyclic change of microstrain in milled Cu samples will be discussed in Sec. IV.

2. Lattice parameter

The lattice parameters of the milled nc Cu were calculated from the intensity peak centroid positions by the weighted least-square method in order to minimize the calculation error. The peak positions were calibrated by the external standard method using a pure Si polycrystal to minimize the systemic error. The detailed procedure of the lattice parameters determination was described in Ref. 24.

The measured lattice parameter of the milled Cu samples are found to be very close to the equilibrium value of the coarse-grained Cu ($a_0=3.615$ Å), and remain unchanged against the milling time. Evident variations of the lattice parameters have been observed in nc Ni_3P, Fe_2B, and Se made by means of the NAS method:[24,29,30] the lattice parameter a is enhanced while c is depressed. Moreover, for the milled nc

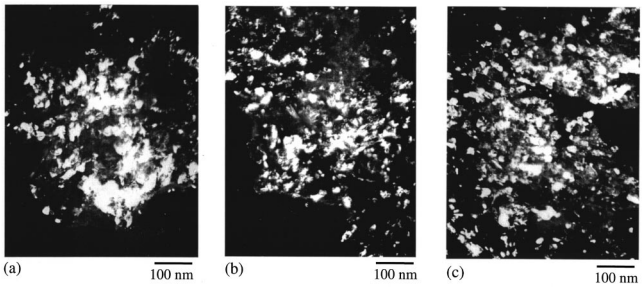

FIG. 3. TEM dark-field images of the milled Cu particles with the milling times of 2 (a), 20 (b), and 100 h (c), respectively.

Si, Ge, Se, and Nb_3Sn, evident lattice expansions were also found.[20–22,31]

The lattice expansion can be explained from a thermodynamic point of view.[32] With respect to that of the infinite large crystal, the free energy of a crystallite, of which the dimension is D, will be increased by $\Delta G(T,D)=4\Omega\gamma/D$, where Ω is the atomic volume of the grain and γ is the interfacial free energy. Therefore, a reduction of the grain size will enlarge the free energy of the crystallites and consequently raise the equilibrium solute solubility in the crystal lattice. In a pure element system, point defects and vacancies are possible ''solutes.'' Introduction of more point defects or vacancies in the crystal lattice would disturb the lattice structure, resulting in a lattice expansion. However, from the present result, the lattice parameter of the milled nc Cu was nearly unchanged during the milling process. Moreover, in the literature, no evident lattice expansion was observed in the pure nc metal produced by mechanical attrition. This may be due to the strong ability of defect recovery of pure metals and the excess points defects can not exist in the lattice of crystal.

3. TEM and composition analyses

The TEM technique was employed to obtain further information about the morphology and microstructure of the milled Cu powders. From TEM observations, we found that the milled Cu particles are irregular thin flat-shaped, and their sizes range from micrometers to submicrometers. The milled particles are polycrystalline consisting of a large number of nanometer-sized grains. Figures 3(a)–3(c) show TEM dark-field images of the milled Cu particles with the milling times of 2, 20, and 100 h, respectively. One can see that, at the beginning of the milling ($t=2$ h), the distribution of the grain size is rather inhomogeneous, meaning that partial deformation takes place in the milled powders by attrition [Fig. 3(a)]. When $t\geqslant 20$ h, however, the grain size distribution is relatively narrow [Figs. 3(b) and 3(c)], which indicates the extended milling produces a uniform comminution. The grain size estimated from TEM pictures is about 12 nm when $t=100$ h, agreeing with the value calculated from XRD broadening peaks.

Since the Cu powders underwent a long period of milling, contamination from milling media and atmosphere was inevitable. Wet chemical analysis shows that the Fe content reaches a maximum of 0.50 wt. % after 100 h of milling,

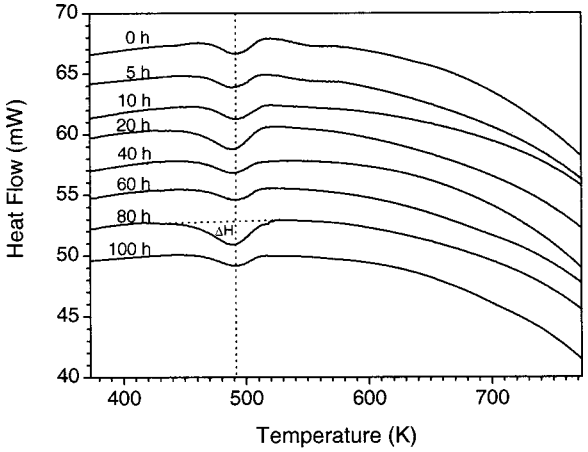

FIG. 4. DSC scans at the heating rate of 10 K min^{-1} for the milled nc Cu samples. Integration of the signal deviating from the baseline gives the stored enthalpy ΔH.

indicating that the contamination from the milling media is minor. This is because at the beginning of milling, a thin Cu layer was formed and coated the surface of the balls and vial, which prevented the further introduction of Fe from the balls and vial. The O analysis indicates that less than 1-at. % O exists in the dispersion milled for 100 h.

B. Thermal properties

The thermal properties of the milled Cu were examined by means of DSC measurement from 373 to 773 K, with a constant heating rate of 10 K min^{-1}. Figure 4 shows the DSC scans for the milled Cu samples. It can be seen that, when $t\leqslant 5$ h an exothermic peak at about 490 K with a long tail appears in the DSC curves, but when $t\geqslant 10$ h, the long tail fades away. Moreover, the exothermic peak position is unchanged versus the milling time. Similar results were found in milled Fe powders.[11]

By integrating the area of the exothermic peak (for the samples when $t\leqslant 5$ h, the integration includes the part of the long tail), we obtained the stored enthalpy ΔH, as shown in Fig. 5. ΔH is observed to possess two maxima at 20 h

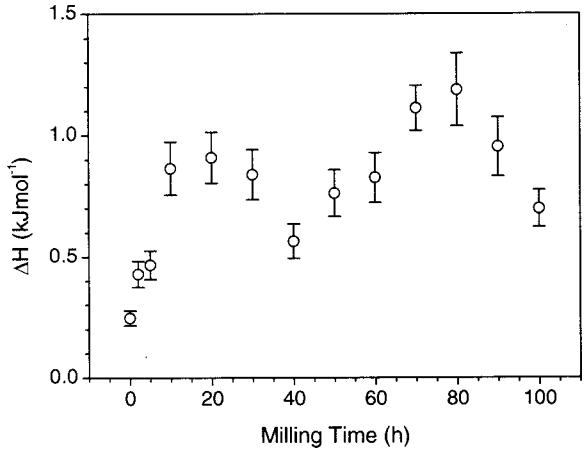

FIG. 5. The stored enthalpy ΔH in the ball-milled nc Cu vs the milling time.

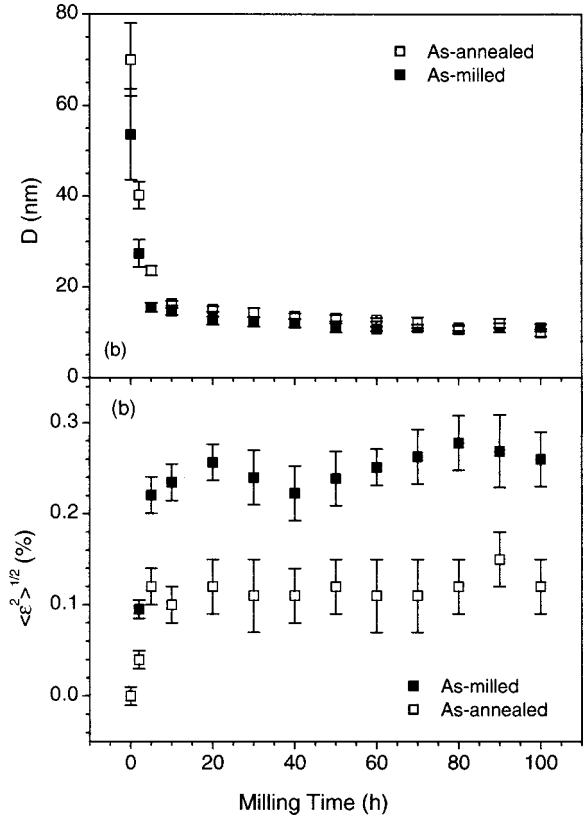

FIG. 6. The mean grain size (a) and microstrain (b) of the as-annealed (open square) and as-milled (solid square) Cu samples.

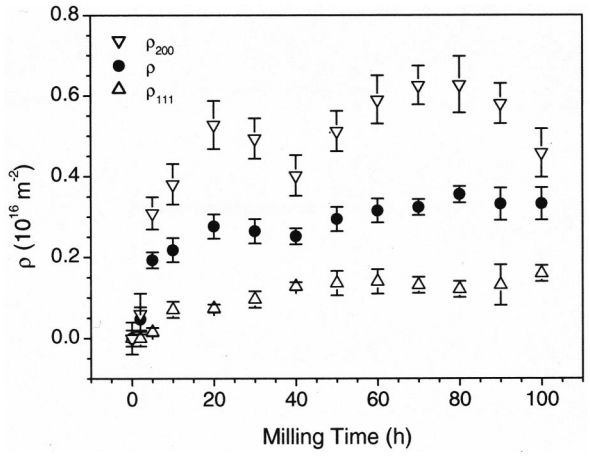

FIG. 7. The mean dislocation density and the dislocation densities along the ⟨200⟩ and ⟨111⟩ directions for the milled Cu samples.

$(0.91 \pm 0.10\ \mathrm{kJ\,mol^{-1}})$ and at 80 h $(1.19 \pm 0.15\ \mathrm{kJ\,mol^{-1}})$ and decrease largely with the further milling to 40 h $(0.57 \pm 0.07\ \mathrm{kJ\,mol^{-1}})$ and 100 h $(0.70 \pm 0.08\ \mathrm{kJ\,mol^{-1}})$, respectively. In literature, only one maximum value of ΔH was observed in the milled nc AlRu, Ru,[6] Ni,[8] W,[9] Fe,[11] etc, which is similar to the variation of ΔH in the milling stage of 0–40 h in the present experiment.

An XRD analysis was used to examine the microstructural changes of the milled Cu after DSC annealing. Figures 6(a) and 6(b) show the plots of the mean grain size and microstrain of both annealed and milled Cu samples. It is clear that, after DSC annealing, the microstrain are decreased remarkably, suggesting that defects recovered after annealing. However, the grain growth only takes place at the early stage of milling ($t \leqslant 5$ h), which corresponds to the long tail in the DSC curves; when $t \geqslant 10$ h, very slight increments in grain sizes (1–2 nm) after DSC measurements were observed. The lattice parameter of the annealed Cu samples was found to be near the equilibrium value, and remained unchanged compared to those of as-milled sample. The absence of grain growth was further confirmed by the TEM observation.

The above results indicate that the exothermic peak in the DSC curves when $t \geqslant 10$ h is primarily originates from a relaxation of defects with a minor contribution from grain growth. Similar results were found in the milled Fe powders.[11] While in the milled Ni and Ru, evident grain growth and strain release were observed after DSC runs.[8] Moreover, the present results imply that the grains of the milled Cu are very stable: when $t \geqslant 10$ h, the grain growth temperature is larger than 773 K. In literature, the grain growth temperatures of nc Cu made by means of ED and SPD methods are about 348 and 434 K, respectively,[27,33] while for the nc Al prepared by mechanical attrition and nc Au by consolidation of UFPs, the grain growth took place only at rather high temperatures.[34,35] The stable grain size in the milled nc Cu might be attributed to either the contamination from the milling process or the large lattice strain that hinder the grain growth process.[27,36]

IV. DISCUSSION

From the above analyses, it is clear that the mechanical attrition process of Cu powders can be separated into two stages: grain refinement and grain steady state. During the former period, large amount of defects (such as GB's, dislocations, point defects, etc.) were introduced into the samples, causing the increases of the microstrain and the stored enthalpy. During the latter period, however, cyclic changes (decrease-increase-decrease) of the microstrain and the stored enthalpy were observed, which means that the microstructural cyclic variation of the milled Cu occurs, even though D stays constant.

A. Dislocation density

For milled samples subjected to severe plastic deformation, dislocations are the main defects besides GB's, of which density ρ_{hkl} can be represented in terms of D_{hkl} and $\langle \varepsilon_{hkl}^2 \rangle^{1/2}$ by[37]

$$\rho_{hkl} = (\rho_D \rho_s)^{1/2} = 2\sqrt{3} \langle \varepsilon_{hkl}^2 \rangle^{1/2} / (D_{hkl}\, b), \tag{2}$$

where b is the Burgers vector of dislocations, and is equal to 0.25562 nm for Cu. The calculated dislocation densities of the as-milled Cu samples are shown in Fig. 7. It is clearly seen that the dislocation also exhibits features similar to the microstrain during the entire milling process. The maximum dislocation density in present work $(0.63 \times 10^{16}\ \mathrm{m^{-2}})$ is comparable to the dislocation density limits in metals

TABLE I. A list of the mean dislocation densities of the as-milled (ρ_{milled}) and as-annealed Cu samples (ρ_{annealed}), the elastic energy release of dislocation (ΔE_{DS}), the GB enthalpy release (ΔE_{GB}), and the GB enthalpy release per area ($\Delta\gamma_{\text{GB}}$) for the milled Cu samples.

Milling time (h)	ρ_{milled} (10^{16} m^{-2})	ρ_{annealed} (10^{16} m^{-2})	ΔE_{DS} (10^{-2} kJ mol^{-1})	ΔE_{GB} (10^{-2} kJ mol^{-1})	$\Delta\gamma_{\text{GB}}$ (Jm^{-2})
0	0	0	0	24.64	—
2	0.05	0.01	0.34	42.51	—
5	0.19	0.07	1.07	45.64	—
10	0.22	0.08	1.20	85.23	0.29
20	0.28	0.11	1.42	89.45	0.26
30	0.26	0.10	1.35	82.53	0.24
40	0.25	0.11	1.19	55.33	0.16
50	0.29	0.12	1.39	74.87	0.19
60	0.32	0.12	1.62	80.99	0.20
70	0.32	0.12	1.66	109.59	0.28
80	0.36	0.15	1.71	117.12	0.29
90	0.33	0.17	1.33	93.99	0.24
100	0.33	0.16	1.45	68.41	0.17

achieved by plastic deformation (10^{13} m^{-2} for screw dislocations and 10^{16} m^{-2} for edge dislocations).[38] The average dislocation densities of the as-milled and as-annealed Cu are also listed in Table I.

It is reported that within the steady-state milling, the dislocation multiplication rate is balanced by the annihilation rate.[3] However, from the present results, the dislocation densities are not simply steady. Usually, in conventional polycrystalline materials, the GB's are thought of as barriers to the dislocation motion which can cause dislocation pileup at GB's, and the variation of the GB structure and/or energetic state can influence the amount of dislocations piled up at GB's. Therefore, the cyclic change of the dislocation density of milled Cu within the $D_{\min}$ stage hints at a cyclic change of the GB structure.

B. Estimation of the GB enthalpy

From Sec. III B one can see that the exothermic peaks in the DSC curves when $t \geqslant 10$ h correspond mainly to the release of enthalpy stored in the heavily deformed Cu samples. The enthalpy release mainly originates from the recovery of defects and includes two components: nonequilibrium lattice defects in grains and GB's. The former contribution is mainly the elastic energy of dislocations in grains, and can be considered as a bulk term. The latter originates mainly from structural and compositional deviations in the GB region from the inner part of the grains, and is a surface term.

In plastically deformed materials, the energy of elastic strain field of dislocations per unit volume E_{DS} can be written as

$$E_{\text{DS}} = AGb^2\rho \ln(R_e/r_0), \tag{3}$$

where $A = 1/4\pi$ for screw dislocation and $A = 1/4\pi(1-\nu)$ for the edge dislocation; here ν is Poisson's ratio. G is the shear modulus. R_e and r_0 are the outer and inner cutoff radii of the dislocations, respectively. In most cases, $r_0 = b$ is taken. R_e, in normal materials, is much smaller than the grain size, while in nc materials, it would far exceed D; therefore, D was considered as the outer cutoff radius of the dislocations. The interaction energy of the dislocations can be neglected since, for nc materials, despite the rather high dislocation density, individual grains contain only a few dislocations.[39]

Assuming that the grains contain equal numbers of screw and edge dislocations, the constant A must be averaged for the two types of dislocations. The value of G and υ for Cu was taken as 4.68×10^{10} N m^{-2} and 0.364, respectively.[40] Placing the difference between ρ_{milled} and ρ_{annealed} into Eq. (3), the elastic energy release of the dislocations for the milled Cu after DSC annealing, ΔE_{DS}, can be determined, as plotted in Fig. 8 and listed in Table I. ΔE_{DS} also possesses a cyclic change within the $D_{\min}$ stage, while it only yields very small fraction of ΔH, suggesting that most of ΔH originates from the GB enthalpy release.

Separating ΔE_{DS} from ΔH, one can get obtain the release of GB enthalpy, ΔE_{GB}, as shown in Fig. 8. It can be estab-

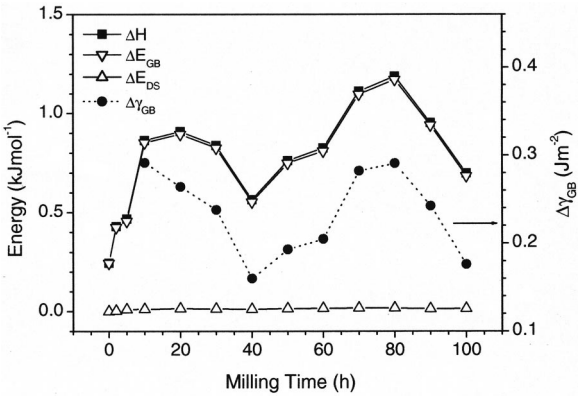

FIG. 8. The stored enthalpy ΔH, the GB enthalpy release ΔE_{GB}, and the elastic energy release of dislocation ΔE_{DS} as well as the GB enthalpy release per area $\Delta\gamma_{\text{GB}}$ of the milled Cu samples.

lished that ΔE_{GB} yields a dominant part in ΔH. Atoms at GB's may have slightly different coordination numbers compared to those in grains interiors.[41] Due to the increase of the atomic distances in the boundaries, the bonds are also distorted. Upon annealing, structural relaxation may first occur in GB regions when the broken bonds annihilate, releasing the energy stored at GB's.

When $t \geqslant 10$ h, D is nearly unchanged after DSC annealing. So we can only estimate the enthalpy release of the GB's per area, $\Delta\gamma_{GB}$ ($=\gamma_{GB}^{milled}-\gamma_{GB}^{annealed}$, γ_{GB}^{milled} and $\gamma_{GB}^{annealed}$ are the GB enthalpy of the as-milled and as-annealed Cu), by correlating ΔE_{GB} with the total surface of GB per mole, as shown in Fig. 8 and listed in Table I. With an increase of the milling time within the steady-state milling, $\Delta\gamma_{GB}$ decreases from 0.29 J m^{-2} (10 h) to 0.16 J m^{-2} (40 h), then increases to a maximum value of 0.29 J m^{-2} (80 h) and decreases again to 0.17 J m^{-2} (100 h). Supposing that $\gamma_{GB}^{annealed}$ of the milled samples are the same, one can deduce that γ_{GB}^{milled} possesses a decrease-increase-decrease variation within the stage of steady-state milling, that is, a GB softening-hardening-softening cyclic change, which agrees with the cyclic variation of the dislocation density. In the literature, a decreased GB enthalpy was reported for the nc Fe during the milling stage of D_{min}.[11] In nc Ni-P (Ref. 42) and Se (Ref. 43) crystallizing from their amorphous states, as well as TiO_2 made by consolidation of UFP's,[44] a decrease of GB enthalpy with a reduction of D was observed. The present results, moreover, indicate that even though D stays unchanged, the GB enthalpy can change cyclically with milling process.

In the literature, a cyclic crystalline-amorphous transformation during mechanical alloying was observed in Co-Ti and Al-Zr systems.[45,46] The authors excluded the influences of the contamination introduction and/or the increase of the vial's temperature during milling, and deduced that the cyclic increase and decrease of the lattice imperfections in the milled samples may play a dominant role in the cyclic phase transformation. This agrees with present results. In addition, the cyclic change of the GB structure of the milled Cu within the steady-state milling hints at one kind of the deformation mechanisms of nc materials, e.g., the GB sliding. GB sliding has been observed in many cases at high temperatures leading to superplasticity behavior. GB sliding can also be achieved at very small grain sizes and low temperature by a diffusion flow of atoms along the inter-crystalline interfaces.[47] During GB sliding, self-organization and rotation of grains can occur. The cyclic rotation of grains may cause the observed cyclic change of the microstrain (dislocation density). The cyclic change of the orientation relationship between the neighboring grains may result in a GB softening-hardening-softening change. In literature, *in situ* TEM deformation studies also observed the clear GB sliding and rotation of 10-nm grain size samples.[48–50] More accurate evidence of the GB sliding and grain rotation in the milled nc Cu needs to be provided to understand the natural structure change of the GB's.

V. CONCLUSION

Quantitative XRD and DSC results of microstructural evolution and thermal properties in nc Cu during mechanical attrition indicated that, in the early stage of milling, grain refinement occurs accompanied by an introduction of defects, leading to evident increases of the microstrain and the stored enthalpy. During the stage when the grain size is D_{min}, decrease-increase-decrease cyclic changes were found for the microstrain and the stored enthalpy. The lattice parameter stays nearly unchanged during the entire milling period. The above phenomena can be reasonably interpreted by the GB softening-hardening-softening variation during steady-state milling supported by a clear decrease-increase-decrease change of the GB enthalpy. A possible deformation mechanism of nc materials during steady-state milling, GB sliding, was proposed and needs to be verified further.

ACKNOWLEDGMENTS

Financial supports from the Chinese Academy of Sciences, Max Planck Society of Germany (MPG Partner Group Project), the National Science Foundation of China (Grant Nos. 59625101 and 59771019), and the Ministry of Science & Technology (G1999064505) are acknowledged.

*Author to whom all correspondence should be addressed. FAX: +49-711-689-3312. Email address: y.h.zhao@mf.mpg.de

[1] H. Gleiter, Prog. Mater. Sci. **33**, 233 (1989).
[2] C. C. Koch, Nanostruct. Mater. **2**, 109 (1993); **9**, 13 (1997).
[3] H. J. Fecht, in *Nanophase Materials*, edited by G. C. Hadjipanayis and R. W. Siegel (Kluwer, Dordrecht, 1994), p. 125; Nanostruct. Mater. **6**, 33 (1995).
[4] A. W. Weeber and H. Bakker, Physica B **153**, 93 (1988).
[5] C. Suryanarayana, Prog. Mater. Sci. **46**, 1 (2001).
[6] E. Hellstern, H. J. Fecht, Z. Fu, and W. L. Johnson, J. Appl. Phys. **65**, 305 (1989); E. Hellstern, H. J. Fecht, Z. Fu, and W. L. Johnson, in *Multicomponent Diffractive Microstructures*, edited by L. G. McCandlish, D. G. Polk, R. W. Siegel, and B. H. Rear, MRS Symposia Proceedings No. 132 (Materials Research Society, Pittsburgh, 1989), p. 137.
[7] H. J. Fecht, E. Hellstern, Z. Fu, and W. L. Johnson, Adv. Powder Metall. **1**, 111 (1989); H. J. Fecht, E. Hellstern, Z. Fu, and W. L. Johnson, Metall. Mater. Trans. A **21**, 2333 (1990).
[8] J. Eckert, J. C. Holzer, C. E. Krill III and W. L. Johnson, J. Mater. Res. **7**, 1751 (1992); J. Eckert, J. C. Holzer, C. E. Krill III and W. L. Johnson, Mater. Sci. Forum **88–90**, 505 (1992).
[9] D. Oleszak and P. H. Shingu, J. Appl. Phys. **79**, 2975 (1996).
[10] H. H. Tian and M. Atzmon, Acta Mater. **47**, 1255 (1999).
[11] Y. H. Zhao, H. W. Sheng, and K. Lu, Acta Mater. **49**, 365 (2001).
[12] X. Zhang, H. Wang, J. Narayanand, and C. C. Koch, Acta Mater. **49**, 1319 (2001).
[13] P. H. Shingu, B. Huang, S. R. Niskitani and S. Nasu, Suppl. Tans. JIM **29**, 3 (1988).
[14] J. Eckert, J. C. Holzer, C. E. Krill III, and W. L. Johnson, J. Mater. Res. **7**, 1980 (1992).
[15] R. B. Schwarz, P. B. Desch, S. Srinivasan, and P. Nash, Nanostruct. Mater. **1**, 37 (1992).
[16] M. L. Trudeau, R. Schulz, D. Dussault, and A. V. Neste, Phys.

Rev. Lett. **64**, 99 (1990); M. L. Trudeau, J. Y. Huot, R. Schulz, D. Dussault, A. V. Neste, and G. L. Espérance, Phys. Rev. B **45**, 4626 (1992).
[17] C. Bansal, B. Fultz, and W. L. Johnson, Nanostruct. Mater. **4**, 919 (1994).
[18] B. Huang, R. J. Perez, P. J. Crawford, A. A. Sharif, S. R. Nutt, and E. J. Lavernia, Nanostruct. Mater. **5**, 545 (1995).
[19] I. Börner and J. Eckert, Mater. Sci. Eng., A. **226–228**, 541 (1997).
[20] E. Gaffet and M. Harmelin, J. Less-Common Met. **157**, 201 (1990).
[21] Y. H. Zhao, Z. H. Jin, and K. Lu, Philos. Mag. Lett. **79**, 747 (1999).
[22] E. Gaffet, Mater. Sci. Eng., A **136**, 161 (1991).
[23] *Powder Diffraction File*, (Joint Committee on Powder Diffraction Standards, Swarthmore, PA, 1990), No. 04-0836.
[24] Y. H. Zhao, K. Zhang, and K. Lu, Phys. Rev. B **56**, 14 322 (1997).
[25] K. Zhang, I. V. Alexandrov, R. Z. Valiev, and K. Lu, J. Appl. Phys. **80**, 5617 (1996).
[26] J. A. Eastman, M. R. Fitzsimmons, and L. J. Thompson, Philos. Mag. B **66**, 667 (1992).
[27] L. Lu, N. R. Tao, L. B. Wang, B. Z. Ding, and K. Lu, J. Appl. Phys. **89**, 6408 (2001).
[28] S. Enzo, M. Sampoli, G. Cocco, L. Schiffini, and L. Battezzati, Philos. Mag. B **59**, 169 (1989).
[29] M. L. Sui and K. Lu, Mater. Sci. Eng., A **179–180**, 541 (1994).
[30] X. D. Liu, K. Lu, B. Z. Ding, and Z. Q. Hu, Nanostruct. Mater. **2**, 581 (1993).
[31] Y. S. Cho and C. C. Koch, Mater. Sci. Eng., A **141**, 139 (1991).
[32] K. Lu and M. L. Sui, J. Mater. Sci. Technol. **9**, 419 (1993).
[33] J. Lian, R. Z. Valiev, and B. Baudelet, Acta Metall. Mater. **43**, 4165 (1995).
[34] F. Zhou, J. Lee and E. J. Lavernia, Scr. Mater. **44**, 2013 (2001).
[35] T. Inami, S. Okuda, H. Maeta, and H. Ohtsuka, Mater. Trans., JIM **39**, 1029 (1998).
[36] B. Günther, A. Kumpmann, and H. D. Kunze, Scr. Metall. Mater. **27**, 83 (1992).
[37] G. K. Williamson and R. E. Smallman, Philos. Mag. **1**, 34 (1956); R. E. Smallman and K. H. Westmacott, *ibid.* **2**, 669 (1957).
[38] U. Essmann and H. Mughrabi, Philos. Mag. A **40**, 40 (1979).
[39] Á. Révész, T. Ungár, A. Borbély, and J. Lendvai, Nanostruct. Mater. **7**, 779 (1996).
[40] *American Institute of Physics Handbook*, 2nd ed. edited by D. E. Gray (McGraw-Hill, New York, 1963).
[41] E. A. Stern, R. W. Siegel, M. Newville, P. G. Sanders, and D. Haskel, Phys. Rev. Lett. **75**, 3874 (1995).
[42] K. Lu, R. Lück, and B. Predel, J. Non-Cryst. Solids **156–158**, 589 (1993); K. Lu, Nanostruct. Mater. **2**, 643 (1993).
[43] K. Lu and N. X. Sun, Philos. Mag. Lett. **75**, 389 (1997).
[44] C. D. Terwilliger and Y. M. Chiang, in *Nanophase and Nanocomposite Materials*, edited by S. Romameni, J. C. Parker, and G. J. Thomas, MRS Symposia Proceedings No. 286 (Materials Research Society, Pittsburgh, 1993), p. 15.
[45] M. Sherif El-Eskandarany, K. Akoi, K. Sumiyama, and K. Suzuki, Appl. Phys. Lett. **70**, 1679 (1997); Scr. Mater. **36**, 1001 (1997).
[46] M. Sherif El-Eskandarany, K. Akoi, K. Sumiyama, and K. Suzuki, Metall. Mater. Trans. A **30**, 1877 (1999); K. Akoi, M. Sherif El-Eskandarany, K. Sumiyama, and K. Suzuki, Mater. Sci. Forum **269–272**, 119 (1998).
[47] J. Karch, R. Birringer, and H. Gleier, Nature (London) **330**, 556 (1987).
[48] W. W. Milligan, S. A. Hackney, M. Ke, and E. C. Aifantis, Nanostruct. Mater. **2**, 269 (1993).
[49] S. A. Hackney, M. Ke, W. W. Milligan, and E. C. Aifantis, in *Processing and Properties of Nanocrystalline Materials*, edited by C. Suryanarayana, J. Singh and F. H. Froes (TMS, 1996), p. 421.
[50] M. Ke, S. A. Hackney, W. W. Milligan, and E. C. Aifantis, Nanostruct. Mater. **5**, 689 (1995).